Exclusive deuteron electrodisintegration with polarized electrons and a polarized target

Hartmuth Arenhövel
Institut für Kernphysik, Johannes Gutenberg-Universität, D-6500 Mainz, Germany

Winfried Leidemann
Dipartimento di Fisica, Istituto Nazionale di Fisica Nucleare, Gruppo Collegato di Trento, Università di Trento, I-38050 Povo, Italy

Edward L. Tomusiak
Department of Physics and Saskatchewan Accelerator Laboratory, University of Saskatchewan, Saskatoon, Canada S7N 0W0
(Received 3 February 1992)

Exclusive electrodisintegration of the deuteron using a polarized beam and an oriented target is systematically investigated in a nonrelativistic framework. The structure functions are expanded in terms of Legendre functions whose coefficients are quadratic forms in the electric and magnetic multipole moments. Their experimental separation by specific experimental settings is outlined. The structure functions are studied with respect to their sensitivity to the potential model, to subnuclear degrees of freedom, and to electromagnetic form factors in different kinematical regions.

PACS number(s): 25.10.+s, 24.70.+s, 25.30.Fj, 13.40.Fn

I. INTRODUCTION

In a recent paper [1] (henceforth called I) we have initiated by considering first the more simple inclusive process $^2\vec{\mathrm{H}}(\vec{e},e')$ a systematic study of polarization effects in deuteron electrodisintegration utilizing polarized electrons and/or polarized targets. The general purpose of this study is to reveal to what extent the use of polarized electrons and/or polarized targets will allow a more detailed investigation of the dynamical features of the nuclear system than is possible without the use of polarization. In particular, we want to see how the various polarization observables are affected by the NN interaction model, by subnuclear effects like meson and isobar degrees of freedom, and by the choice of electromagnetic nucleon and meson-exchange current form factors.

With the present work we will continue this study by looking at the exclusive process $^2\mathrm{He}(\vec{e},e'N)N$ of deuteron electrodisintegration. In the past, this process has been investigated theoretically for unpolarized beams and targets by various authors in order to study either the deuteron wave function [2,3] and relativistic and off-shell effects [4,5] in the quasifree region or the effects of meson-exchange currents and isobar configurations [6]. Furthermore, the possibility of determining the charge form factor of the neutron G_{En} from $^2\vec{\mathrm{H}}(\vec{e},e'n)p$ using a vector polarized deuteron target has been discussed in [7,8]. A first systematic survey on the structure functions without beam and target polarization has been given in Ref. [9]. However, such a survey covering the case when both beam and target are polarized is still missing.

As in I we are interested in the general aspects and dynamical properties of the two-body system, e.g., NN potential model sensitivities and the importance of subnuclear degrees of freedom (d.o.f). Compared to the integral quantities, namely, the form factors of the inclusive process, we expect for the exclusive reaction a greater sensitivity of the observables, i.e., the structure functions, to the aforementioned dynamical properties, since they contain interference terms between contributions of different partial waves of the final n-p states. Whereas the inclusive deuteron breakup depends on only 10 form factors the much more complex exclusive process $^2\vec{\mathrm{H}}(\vec{e},e'N)N$ is governed by 41 structure functions.

In Sec. II we briefly review the formulas required for describing the $^2\vec{\mathrm{H}}(\vec{e},e'N)N$ process starting from the general formalism of Ref. [8]. We will still leave out the discussion of the polarization of the reaction products, i.e., the proton and neutron. This will be reserved for the last part of our systematic study. The above-mentioned 41 structure functions are given as Hermitian forms of the t-matrix elements, i.e., the charge and transverse current matrix elements between the deuteron bound state and the continuum n-p state. Using the multipole expansion of the t matrix, the angular dependence of the structure functions can be separated by expanding them in terms of Legendre functions whose coefficients are quadratic forms of the reduced electric and magnetic transition multipole matrix elements.

The various polarization asymmetries with respect to beam and target polarization will be given in Sec. III. There we show how the structure functions can be separated by choosing appropriate experimental conditions. Finally, we study in Sec. IV the structure functions in various kinematical regions. These regions are selected to represent different areas of sensitivities to the final-

state interaction and to interaction currents mediated by meson exchange and Δ-degrees of freedom. For the calculation of the structure functions we use the same nonrelativistic framework as described in I with realistic NN potential models, meson-exchange currents (MEC), and isobar configurations (IC).

II. FORMALISM

The starting point of the formal discussion is the differential cross section for the coincidence reaction which includes both beam and target polarizations as given in Ref. [8],

$$\begin{aligned}\frac{d^3\sigma}{dk_2^{\rm lab}d\Omega_e^{\rm lab}d\Omega_{np}^{\rm c.m.}}=c\Big[&\rho_L f_L+\rho_T f_T+\rho_{LT}f_{LT}\cos\phi+\rho_{TT}f_{TT}\cos2\phi+h\rho'_{LT}f'_{LT}\sin\phi\\&+P_1^d\Big[(\rho_L f_L^{11}+\rho_T f_T^{11})d^1_{10}(\theta_d)\sin(\phi-\phi_d)\\&\quad+\sum_{M=-1}^{1}(\rho_{LT}f_{LT}^{1M}\sin\xi_M+\rho_{TT}f_{TT}^{1M}\sin\psi_M)d^1_{M0}(\theta_d)\Big]\\&+P_2^d\Big[\sum_{M=0}^{2}(\rho_L f_L^{2M}+\rho_T f_T^{2M})d^2_{M0}(\theta_d)\cos[M(\phi-\phi_d)]\\&\quad+\sum_{M=-2}^{2}(\rho_{LT}f_{LT}^{2M}\cos\xi_M+\rho_{TT}f_{TT}^{2M}\cos\psi_M)d^2_{M0}(\theta_d)\Big]\\&+hP_1^d\Big[\rho'_T\sum_{M=0}^{1}f'^{1M}_T\cos[M(\phi-\phi_d)]d^1_{M0}(\theta_d)+\rho'_{LT}\sum_{M=-1}^{1}f'^{1M}_{LT}\cos\xi_M d^1_{M0}(\theta_d)\Big]\\&+hP_2^d\Big[\rho'_T\sum_{M=1}^{2}f'^{2M}_T\sin[M(\phi-\phi_d)]d^2_{M0}(\theta_d)+\rho'_{LT}\sum_{M=-2}^{2}f'^{2M}_{LT}\sin\xi_M d^2_{M0}(\theta_d)\Big]\Big]\\=&S(h,P_1^d,P_2^d)\ ,\end{aligned}\tag{1}$$

with

$$c=\frac{\alpha}{6\pi^2}\frac{k_2^{\rm lab}}{k_1^{\rm lab}q_\nu^4}\ ,\tag{2}$$

$$\xi_M=M(\phi-\phi_d)+\phi\ ,\tag{3}$$

$$\psi_M=M(\phi-\phi_d)+2\phi\ .\tag{4}$$

The scattering geometry is illustrated in Fig. 1. Here, θ and ϕ [$\Omega_{np}^{\rm c.m.}=(\theta,\phi)$] denote the spherical angles of the relative final-state n-p momentum $\mathbf{k}$ in the final n-p c.m. system. Note that only longitudinally polarized electrons are considered. The quantities[1] $\rho^{(\prime)}_{\mu'\mu}$ describe the virtual photon density matrix [$(\mu'\mu)=(00)$, (11), (01), and (-11) correspond to L,T,LT, and TT, respectively], h is the degree of longitudinal electron polarization, $k_1^{\rm lab}$ and $k_2^{\rm lab}$ denote the laboratory frame momenta of the initial and the scattered electrons, respectively, while q_ν^2 is the four-momentum transfer squared ($q=k_1-k_2$). The structure functions $f^{(\prime)IM}_{\mu'\mu}$ ($f^{(\prime)00}_{\mu'\mu}\equiv f^{(\prime)}_{\mu'\mu}$) are all calculated in the final n-p c.m. system. This system, which sometimes is also called antilab system, moves in the laboratory with total momentum $\mathbf{q}_{\rm lab}$. Kinematical effects of the boost from the laboratory to the c.m. system are included in the virtual photon density matrix which thus has to be evaluated in the c.m. system leading to

$$\rho_L=\beta^2q_\nu^2\frac{\xi^2}{2\eta}\ ,\quad \rho_{LT}=\beta q_\nu^2\frac{\xi}{\eta}\left[\frac{\xi+\eta}{8}\right]^{1/2}\ ,\tag{5}$$

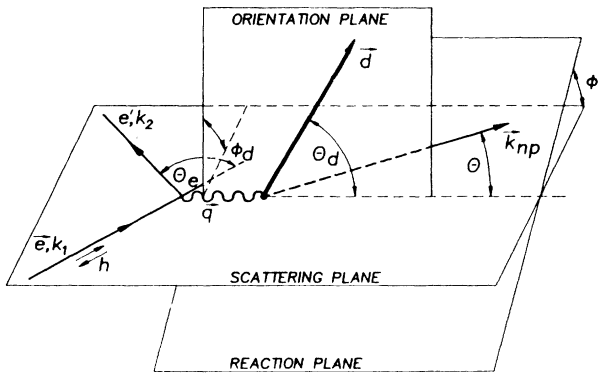

FIG. 1. Geometry of exclusive electron-deuteron scattering with polarized electrons and oriented deuteron target. Relative n-p momentum is denoted by $\mathbf{k}_{np}$ characterized by angles θ and ϕ and deuteron orientation axis by $\mathbf{d}$ characterized by angles θ_d and ϕ_d.

[1]Primed and unprimed quantities, $\rho_{\mu'\mu}$ and $\rho'_{\mu'\mu}$, are here referred to collectively as $\rho^{(\prime)}_{\mu'\mu}$, a similar convention is used for $f^{(\prime)IM}_{\mu'\mu}$.

$$\rho_T=\tfrac{1}{2}q_\nu^2\left[1+\frac{\xi}{2\eta}\right],\quad \rho_{TT}=-q_\nu^2\frac{\xi}{4\eta}, \tag{6}$$

$$\rho'_{LT}=\tfrac{1}{2}\beta q_\nu^2\frac{\xi}{\sqrt{2\eta}},\quad \rho'_T=\tfrac{1}{2}q_\nu^2\left[\frac{\xi+\eta}{\eta}\right]^{1/2}, \tag{7}$$

with

$$\beta=\frac{|\mathbf{q}_{\rm lab}|}{|\mathbf{q}_{\rm c.m.}|},\quad \xi=\frac{q_\nu^2}{\mathbf{q}_{\rm lab}^2},\quad \eta=\tan^2\left[\frac{\theta_e^{\rm lab}}{2}\right], \tag{8}$$

where β expresses the boost from the laboratory to the c.m. system. The deuteron target is characterized by vector and tensor polarization parameters P_1^d and P_2^d, respectively, and by the angles θ_d and ϕ_d describing the direction of the orientation axis $\hat{\mathbf{d}}$ of the polarized deuteron target with respect to the coordinate system associated with the three-momentum transfer $\mathbf{q}$ (see Fig. 1). We would like to remind the reader that $\hat{\mathbf{d}}$ is the axis with respect to which the deuteron density matrix is diagonal. Note that the deuteron density matrix undergoes no change in the transformation from the laboratory to the c.m. system, since the boost is along $\mathbf{q}$ [10].

The structure functions $f_{\mu'\mu}^{(\prime)1M}$ are proportional to either the real or imaginary parts of the quantities

$$v_{\mu'\mu IM}(\theta)=\hat{I}\sqrt{3}\sum_{m_d m_d'}(-)^{1-m_d}\begin{pmatrix}1 & 1 & I\\ m_d & -m_d' & -M\end{pmatrix}\sum_{sm_s}t^*_{sm_s\mu' m_d'}(\theta)t_{sm_s\mu m_d}(\theta), \tag{9}$$

where $t_{sm_s\mu m_d}$ is the reduced transition matrix for the process $d+e\rightarrow np+e'$. Counting all different combinations of $(\mu'\mu IM)$ one finds a total number of 81. However, the corresponding $v_{\mu'\mu IM}$ are not all linearly independent because of the two symmetry relations given in Eqs. (76) and (77) of [8] which follow from parity conservation. The first one

$$v_{-\mu'-\mu I-M}=(-)^{I-M+\mu'-\mu}v_{\mu'\mu IM} \tag{10}$$

eliminates one, namely $v_{0010}=0$, and relates for $|\mu'|+|\mu|+|M|>0$ the $v_{\mu'\mu IM}$ with $M\le 0$ to different ones with $M\ge 0$. Thus there remain 41 complex functions $v_{\mu'\mu 1M}$, namely 27 with $M>0$ and 14 with $M=0$. The second symmetry relation

$$(v_{\mu'\mu IM})^*=(-)^{I+\mu'-\mu}v_{-\mu'-\mu IM} \tag{11}$$

then leads to 41 independent real functions which are related to the above-mentioned 41 structure functions in (1).

In detail one has [8]

$$f_{\mu'\mu}^{IM}(\theta)=\frac{4(-)^{1+\delta_{I0}}}{(1+\delta_{\mu',-\mu})(1+\delta_{M0}\delta_{\mu'\mu})}\mathrm{Re}[i^{-I}v_{\mu'\mu IM}(\theta)], \tag{12}$$

$$f'^{IM}_{\mu'\mu}(\theta)=\frac{4(-)^{\delta_{I0}}}{(1+\delta_{M0}\delta_{\mu'\mu})}\mathrm{Im}[i^{I}v_{\mu'\mu IM}(\theta)]. \tag{13}$$

Reference [8] should be consulted for a detailed description of all the terms in (1). Note that the structure functions depend on θ, the c.m. angle of the relative n-p momentum of the final state, on E_{np}, the n-p final state c.m. energy, and on $\mathbf{q}_{\rm c.m.}$, the c.m. three-momentum transfer.

Incidentally, we would like to mention that at the photon point one has the following relationships between the purely transverse structure functions and (a) the differential cross section $d\sigma_0/d\Omega$ of deuteron photodisintegration for unpolarized photons and unoriented deuterons and (b) the corresponding photon and target asymmetries of the differential cross section [11,12]

$$\frac{d\sigma_0}{d\Omega}=\frac{6M_d}{W_{np}\omega_\gamma}f_T,\quad T_{IM}=\frac{f_T^{IM}}{f_T}, \tag{14}$$

$$T_{IM}^c=\frac{f_T'^{IM}}{f_T},\quad T_{IM}^l=\frac{f_{TT}^{IM}}{f_T}, \tag{15}$$

where M_d, W_{np}, and ω_γ denote, respectively, the deuteron mass, the invariant mass of the final n-p system, and the photon c.m. energy.

In order to have a convenient parametrization of the angular behavior of the structure functions it is useful to expand them in terms of Legendre polynomials or associated Legendre functions. This will also facilitate the analysis of the contributions of the various electric and magnetic transition multipole moments to the different structure functions. To this end we use the multipole expansion for the t matrix as given in I

$$t_{sm_s\mu m_d}(\theta)=(-)^\mu\sqrt{(1+\delta_{\mu 0})}\times\sum_{Lljm_j\lambda}\frac{\hat{l}}{\hat{j}}(1m_dL\lambda|jm_j)\times(l0sm_s|jm_s)\mathcal{O}^{L\mu}(\lambda jls)d^j_{m_jm_s}(\theta), \tag{16}$$

where

$$\mathcal{O}^{L\mu}(\lambda jls)=\sqrt{4\pi}e^{i\delta_\lambda^j}U^j_{ls,\lambda}N^L_\mu(\lambda j), \tag{17}$$

and

$$N^L_\mu(\lambda j)=\delta_{|\mu|1}[E^L(\lambda j)+\mu M^L(\lambda j)]+\delta_{\mu 0}C^L(\lambda j)\ . \tag{18}$$

In complete analogy to what has been done in deuteron photodisintegration (see the appendix of Ref. [11]) one finds first

$$v_{\mu'\mu IM}(\theta)=\sum_K v^K_{\mu'\mu IM}d^K_{M+\mu-\mu',0}(\theta)\ , \tag{19}$$

where the coefficients are given in terms of the multipole moments

$$\begin{aligned} v^K_{\mu'\mu IM}=&(-)^{\mu+M}\sqrt{3}\hat{I}\hat{K}^2\sqrt{(1+\delta_{\mu 0})(1+\delta_{\mu' 0})} \\ &\times\sum_J \hat{J}^2 \begin{pmatrix} J & I & K \\ \mu-\mu' & M & \mu'-\mu-M \end{pmatrix} \sum_{\substack{l\lambda jls \\ L'\lambda' j'l'}} (-)^{L+j'+s}\hat{l}\hat{l}'\hat{j}\hat{j}' \begin{pmatrix} K & l & l' \\ 0 & 0 & 0 \end{pmatrix} \begin{pmatrix} L & L' & J \\ \mu & -\mu' & \mu'-\mu \end{pmatrix} \\ &\times \begin{Bmatrix} j & l & s \\ j' & l' & K \end{Bmatrix} \begin{Bmatrix} L & L' & J \\ j & j' & K \\ 1 & 1 & I \end{Bmatrix} Q^{L'\mu'}(\lambda' j'l's)^* Q^{L\mu}(\lambda jls)\ . \end{aligned} \tag{20}$$

These coefficients have as symmetry properties

$$v^K_{-\mu'-\mu IM}=(-)^I v^K_{\mu'\mu I-M}\ , \tag{21}$$

$$\begin{aligned} (v^K_{\mu'\mu IM})^* &=(-)^{\mu'-\mu}v^K_{\mu\mu' I-M}\ , \\ &=(-)^{I+\mu'-\mu}v^K_{-\mu-\mu' IM}\ , \end{aligned} \tag{22}$$

which follow directly from (10) and (11). A specific consequence of these relations is that $v^K_{\mu-\mu IM}$ for $\mu=-1,0,1$ are real for $I=0$ and 2 and imaginary for $I=1$ and thus lead to the vanishing of f'^{IM}_α for $\alpha=L$ and TT as has been noted already in [8]. We would like to point out that in (19) the vanishing of $v_{\mu'\mu IM}$ at $\theta=0$ and π for $\mu'-\mu\neq M$ is directly evident.

Correspondingly one obtains from (12) and (13) the following expansions of the structure functions:

$$f^{(')IM}_{\mu'\mu}(\theta)=\sum_K f^{(')IM,K}_{\mu'\mu}d^K_{M+\mu-\mu',0}(\theta) \tag{23}$$

with the coefficients

$$f^{IM,K}_{\mu'\mu}=\frac{4(-)^{1+\delta_{I0}}}{(1+\delta_{\mu',-\mu})(1+\delta_{M0}\delta_{\mu'\mu})}\mathrm{Re}(i^{-I}v^K_{\mu'\mu IM})\ , \tag{24}$$

$$f'^{IM,K}_{\mu'\mu}=\frac{4(-)^{\delta_{I0}}}{(1+\delta_{M0}\delta_{\mu'\mu})}\mathrm{Im}(i^{I}v^K_{\mu'\mu IM})\ . \tag{25}$$

Note that the inclusive form factors discussed in I are just given by the ($K=0$) coefficients, i.e.,

$$F^{(')IM}_{\mu'\mu}=\frac{2\pi}{3}f^{(')IM,0}_{\mu'\mu}\ , \tag{26}$$

which corresponds to Eqs. (13), (14), and (19) of I.

III. SEPARATION OF STRUCTURE FUNCTIONS

For the purpose of discussing how the various structure functions can be separated experimentally it is more advantageous to rewrite the cross section as given in (1) in the following form:

$$\begin{aligned} \frac{d^3\sigma}{dk_2^{\mathrm{lab}}d\Omega_e^{\mathrm{lab}}d\Omega_{np}^{\mathrm{c.m.}}}=c\sum_{I=0}^{2}P_I^d\sum_{M=0}^{I}\{&(\rho_L f_L^{IM}+\rho_T f_T^{IM}+\rho_{LT}f_{LT}^{IM}+\cos\phi+\rho_{TT}f_{TT}^{IM}+\cos 2\phi)\cos(M\tilde{\phi}-\delta_{I,1}\pi/2) \\ &-(\rho_{LT}f_{LT}^{IM}-\sin\phi+\rho_{TT}f_{TT}^{IM}-\sin 2\phi)\sin(M\tilde{\phi}-\delta_{I,1}\pi/2) \\ &+h(-)^I[(\rho'_T f'^{IM}_T+\rho'_{LT}f'^{IM}_{LT}-\cos\phi)\sin(M\tilde{\phi}-\delta_{I,1}\pi/2) \\ &+\rho'_{LT}f'^{IM}_{LT}+\sin\phi\cos(M\tilde{\phi}-\delta_{I,1}\pi/2)]\}d^I_{M0}(\theta_d) \end{aligned} \tag{27}$$

with $\tilde{\phi}=\phi-\phi_d$. For the sake of a more compact notation, we have introduced $P_0^d=1$, the original notation $f^{00}_\alpha=f_\alpha$ for $\alpha=L,T,LT$, and TT and for the interference terms new structure functions $f^{(')IM\pm}_\alpha$ ($\alpha=LT$ and TT and $M\geq 0$) the following combinations of the old structure functions:

$$f^{(')IM\pm}_\alpha=\frac{1}{(1+\delta_{M,0})}[f^{(')IM}_\alpha\pm(-)^{I+M}f^{(')I-M}_\alpha] \tag{28}$$

with $\alpha=LT$ or TT. Note that f^{00-}_α, $f^{20,-}_\alpha$, and f^{10+}_α vanish identically. For this reason we will use later in the discussion of the results the notation f_α, f^{10}_α, and f^{20}_α instead of f^{00+}_α, f^{10-}_α, and f^{20+}_α, respectively.

In the absence of beam and target polarization, the four structure functions f_α can be separated choosing different ϕ angles and applying the Rosenbluth separation to determine f_L and f_T. The separation of the additional structure functions in the presence of a polarized beam and/or target can be achieved by exploiting the independence of the parameters h, the longitudinal electron polarization, P_1^d and P_2^d, the deuteron vector and tensor polarization, θ_d and ϕ_d,

the orientation angles of the deuteron polarization axis, and ϕ, the out-of-plane angle. By a proper variation of the polarization parameters h and P_I^d one can first separate the various beam, target, and beam-target asymmetries as defined in [8]

$$S(h,P_1^d,P_2^d)=S_0[1+P_1^d A_d^V+P_2^d A_d^T+h(A_e+P_1^d A_{ed}^V+P_2^d A_{ed}^T)] , \tag{29}$$

where $S_0=S(0,0,0)$ denotes the completely unpolarized differential cross section.

For the asymmetries one obtains from (27) the explicit expressions

$$A_e=\frac{c}{S_0}\rho'_{LT}f'_{LT}\sin\phi , \tag{30}$$

$$\begin{aligned}A_d^V&=\frac{c}{S_0}\sum_{M=0}^{1}[(\rho_L f_L^{1M}+\rho_T f_T^{1M}+\rho_{LT}f_{LT}^{1M\,+}\cos\phi+\rho_{TT}f_{TT}^{1M\,+}\cos2\phi)\sin M\tilde{\phi}\\&\quad+(\rho_{LT}f_{LT}^{1M\,-}\sin\phi+\rho_{TT}f_{TT}^{1M\,-}\sin2\phi)\cos M\tilde{\phi}]d^1_{M0}(\theta_d)\\&=\frac{c}{S_0}\left[(\rho_L f_L^{11}+\rho_T f_T^{11}+\rho_{LT}f_{LT}^{11+}\cos\phi+\rho_{TT}f_{TT}^{11+}\cos2\phi)\sin\tilde{\phi}d^1_{10}(\theta_d)\right.\\&\quad\left.+\sum_{M=0}^{1}(\rho_{LT}f_{LT}^{1M\,-}\sin\phi+\rho_{TT}f_{TT}^{1M\,-}\sin2\phi)\cos M\tilde{\phi}d^1_{M0}(\theta_d)\right] ,\end{aligned} \tag{31}$$

$$\begin{aligned}A_d^T&=\frac{c}{S_0}\sum_{M=0}^{2}[(\rho_L f_L^{2M}+\rho_T f_T^{2M}+\rho_{LT}f_{LT}^{2M\,+}\cos\phi+\rho_{TT}f_{TT}^{2M\,+}\cos2\phi)\cos M\tilde{\phi}\\&\quad-(\rho_{LT}f_{LT}^{2M\,-}\sin\phi+\rho_{TT}f_{TT}^{2M\,-}\sin2\phi)\sin M\tilde{\phi}]d^2_{M0}(\theta_d)\\&=\frac{c}{S_0}\left[(\rho_L f_L^{20}+\rho_T f_T^{20}+\rho_{LT}f_{LT}^{20}\cos\phi+\rho_{TT}f_{TT}^{20}\cos2\phi)d^2_{00}(\theta_d)\right.\\&\quad+\sum_{M=1}^{2}[(\rho_L f_L^{2M}+\rho_T f_T^{2M}+\rho_{LT}f_{LT}^{2M\,+}\cos\phi+\rho_{TT}f_{TT}^{2M\,+}\cos2\phi)\cos M\tilde{\phi}\\&\quad\left.-(\rho_{LT}f_{LT}^{2M\,-}\sin\phi+\rho_{TT}f_{TT}^{2M\,-}\sin2\phi)\sin M\tilde{\phi}]d^2_{M0}(\theta_d)\right] ,\end{aligned} \tag{32}$$

$$\begin{aligned}A_{ed}^V&=\frac{c}{S_0}\sum_{M=0}^{1}[(\rho'_T f'^{1M}_T+\rho'_{LT}f'^{1M\,-}_{LT}\cos\phi)\cos M\tilde{\phi}-\rho'_{LT}f'^{1M\,+}_{LT}\sin\phi\sin M\tilde{\phi}]d^1_{M0}(\theta_d)\\&=\frac{c}{S_0}\{(\rho'_T f'^{10}_T+\rho'_{LT}f'^{10}_{LT}\cos\phi)d^1_{00}(\theta_d)\\&\quad+[(\rho'_T f'^{11}_T+\rho'_{LT}f'^{11\,-}_{LT}\cos\phi)\cos\tilde{\phi}-\rho'_{LT}f'^{11\,+}_{LT}\sin\phi\sin\tilde{\phi}]d^1_{10}(\theta_d)\} ,\end{aligned} \tag{33}$$

$$\begin{aligned}A_{ed}^T&=\frac{c}{S_0}\sum_{M=0}^{2}[(\rho'_T f'^{2M}_T+\rho'_{LT}f'^{2M\,-}_{LT}\cos\phi)\sin M\tilde{\phi}+\rho'_{LT}f'^{2M\,+}_{LT}\sin\phi\cos M\tilde{\phi}]d^2_{M0}(\theta_d)\\&=\frac{c}{S_0}\left[\rho'_{LT}f'^{20}_{LT}\sin\phi d^2_{00}(\theta_d)+\sum_{M=1}^{2}[(\rho'_T f'^{2M}_T+\rho'_{LT}f'^{2M\,-}_{LT}\cos\phi)\sin M\tilde{\phi}+\rho'_{LT}f'^{2M\,+}_{LT}\sin\phi\cos M\tilde{\phi}]d^2_{M0}(\theta_d)\right] .\end{aligned} \tag{34}$$

The various asymmetries are functions of the deuteron orientation angles θ_d and ϕ_d, viz., $\tilde{\phi}$ and the azimuthal or out-of-plane angle ϕ. We will now sketch how one can utilize these variables for the further separation of the different structure functions.

The general functional form of an asymmetry is

$$A^1(\phi,\tilde{\phi},\theta_d)=\sum_{M=0}^{I}\alpha_{IM}(\phi,\tilde{\phi})d^I_{M0}(\theta_d) , \tag{35}$$

where

$$\alpha_{IM}(\phi,\tilde{\phi})=c_{IM}(\phi)\cos M\tilde{\phi}+s_{IM}(\phi)\sin M\tilde{\phi} . \tag{36}$$

The ϕ-dependent functions c_{IM} and s_{IM} have either the form

$$a_0+a_1\cos\phi+a_2\cos2\phi \tag{37}$$

or

$$b_1\sin\phi+b_2\sin2\phi . \tag{38}$$

For a given I the M-dependent pieces α_{IM} can be separated by a proper choice of θ_d. For $I=1$ (vector asymmetries) taking $\theta_d=0$ or $\pi/2$ yields α_{10} or α_{11}, respectively, and for $I=2$ (tensor asymmetries) one may first

choose $\theta_d=0$ yielding directly α_{20}, and then $\theta_d=\pi/4$ and $\pi/2$ from which the remaining two terms α_{21} and α_{22} can be determined. For α_{21} and α_{22} one can also choose $\theta_d=\theta_d^0=\arccos(1/\sqrt{3})$ together with $\tilde{\phi}$ and $\tilde{\phi}+\pi$. Then the sum and difference of the corresponding asymmetries result in α_{21} and α_{22}, respectively.

In the next step in order to separate c_{IM} and s_{IM} one can take first $\tilde{\phi}=0$ giving c_{IM} and then $\tilde{\phi}=\pi/2M$ for $M\neq 0$ which yields directly s_{IM}. The remaining separation of a_n or b_n is then achieved by appropriate choices of ϕ. In a few cases the constant term a_0 in (37) will contain two structure functions in the combination $\rho_L f_L^{IM}+\rho_T f_T^{IM}$. In this case one needs a Rosenbluth separation in addition. This completes the general discussion of how to separate in principle the different structure functions although that might in practice become quite involved.

More details can be found in the Appendix. Since some of the structure functions will need only one or a few different asymmetry measurements while others will require a larger number, we will in particular address the question of how many settings are necessary to separate each of the structure functions.

IV. RESULTS AND DISCUSSION

The various structure functions $f_{\mu'\mu}^{(\prime)IM}$ are calculated within the same nonrelativistic framework that has been used for the form factors of the inclusive process in *I*. It is described in detail in Ref. [6] with the one exception that we do not use the nonrelativistic approximation in the kinematical factors of the T matrix as given in Eq. (61) of Ref. [8] but take instead the relativistic expressions. In the calculation of the t-matrix elements we calculate explicitly all electric and magnetic multipoles up to the order $L=6$. That means we include the final-state interaction in all partial waves up to $j=7$. For the higher multipoles we use the Born approximation for the final state, i.e., no final-state interaction in partial waves with $j\geq 8$ as has been described in Ref. [6]. We would like to remark that for the electric transitions we use the Siegert operators in the convention of [13] except in the case of the Born approximation. In this way the major MEC contribution is incorporated implicitly.

For the deuteron and *n-p* scattering wave functions we use the Nijmegen potential [14] in addition to the potential models employed in I, namely, the Paris [15]. Bonn [16] (*r*-space version), and Argonne V_{14} and V_{28} potentials [17]. The latter explicitly includes Δ degrees of freedom within a coupled-channel (CC) approach. Above pion threshold V_{28} is modified for the $^1D_2$ channel in order to give a better description of this channel as described in Ref. [18]. For the other potential models we use the impulse approximation (IA) for the calculation of the IC [18].

In the current operator we include explicit meson-exchange contributions beyond the Siegert operators, essentially from π and ρ exchange, and isobar contributions. For the electromagnetic form factors of the one-body current we use two models: (i) the dipole fit with the two choices $G_{En}=0$ and $G_{En}=D$ (with $p=5.6$) [19] for the neutron electric form factor and (ii) the Gari-Krümpelmann model (GK) [20]. Finally, for the MEC form factor we consider both cases G_E^V and F_1^V [21]. In detail we will investigate the following effects: the influence of meson-exchange (MEC) and isobar currents (IC), the potential model dependence, and neutron electric (G_{En}) and MEC form factor effects (G_E^V vs F_1^V).

In addition to their dependence on θ, the structure functions $f_{\mu'\mu}^{(\prime)IM}$ are also functions of E_{np} and $\mathbf{q}^2_{\text{c.m.}}$, the relative *n-p* energy and the three-momentum transfer squared, respectively, both in the c.m. system. Since E_{np} and $\mathbf{q}^2_{\text{c.m.}}$ cover a whole plane, we have chose for this exploratory study three different cuts in this plane in order to cover regions with different dynamic properties. We have chosen one cut at a constant low energy $E_{np}=30$ MeV taking momentum transfers of 1,10, and 20 fm^{-2}. The second cut is chosen at a constant intermediate energy $E_{np}=120$ MeV choosing momentum transfers of 2,12, and 25 fm^{-2}. Finally, we have taken the third cut at $E_{np}=240$ MeV, the region of Δ excitation, with momentum transfers of 5, 15, and 30 fm^{-2}. These different kinematic sectors are marked in Fig. 2 where we also introduce a numbering in order to facilitate the following discussion of the results.

A. Current contributions

In order to give a first survey on the size and the characteristic features, we show the "unpolarized" structure functions f_α in Figs. 3–6 in all kinematic sectors calculated using the Paris potential, the dipole parametrization of the nucleon form factors ($G_{En}=0$) and G_E^V for the MEC. The effect of the final-state interaction and of the separate current contributions are also indicated in the figures. The prominent feature of f_L is the forward peak corresponding to proton emission in the direction of the momentum transfer $\mathbf{q}$. This peak becomes very narrow in the quasifree case but broadens considerably if one

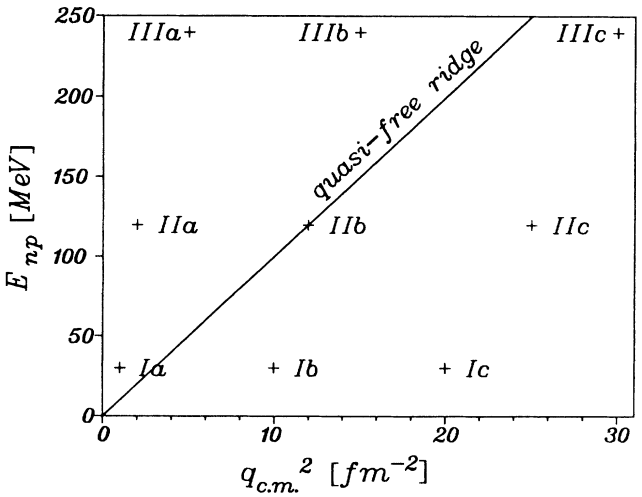

FIG. 2. E_{np}-$\mathbf{q}^2_{\text{c.m.}}$ plane with indication of the location of the quasifree ridge and the kinematic sectors, for which the structure functions have been evaluated.

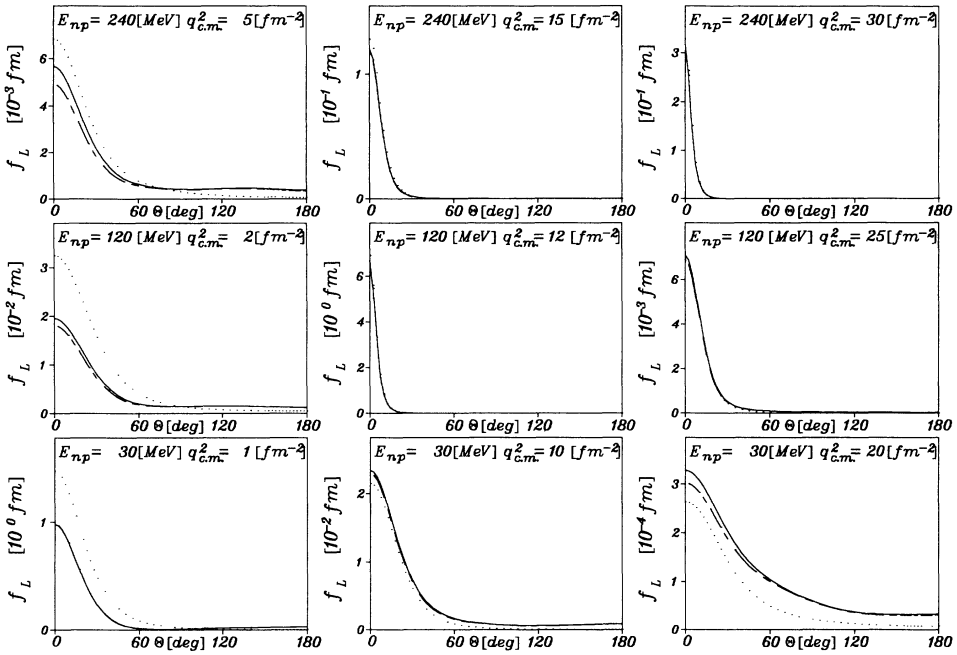

FIG. 3. The structure function f_L calculated using the Paris potential, the dipole nucleon form factor with $G_{En}=0$, and G_E^V for the MEC form factor as function of θ in the kinematic sectors of Fig. 2. Dotted: Born approximation; dashed: normal (N); dash-dotted: N+MEC; full: N+MEC+IC.

moves away from the quasifree ridge. As expected, final-state interaction effects are minimal in the quasifree case but becomes quite strong in the other kinematic sectors since additional interactions are necessary in order to compensate the energy-momentum mismatch. Since meson exchange does not affect the charge density in the nonrelativistic regime, one notices only effects from IC which, however, are small.

The transverse structure function f_T is of the same order though slightly larger than the longitudinal one. As in f_L one notes in the quasifree case a strong and narrow forward peak. In addition, another peak appears in the

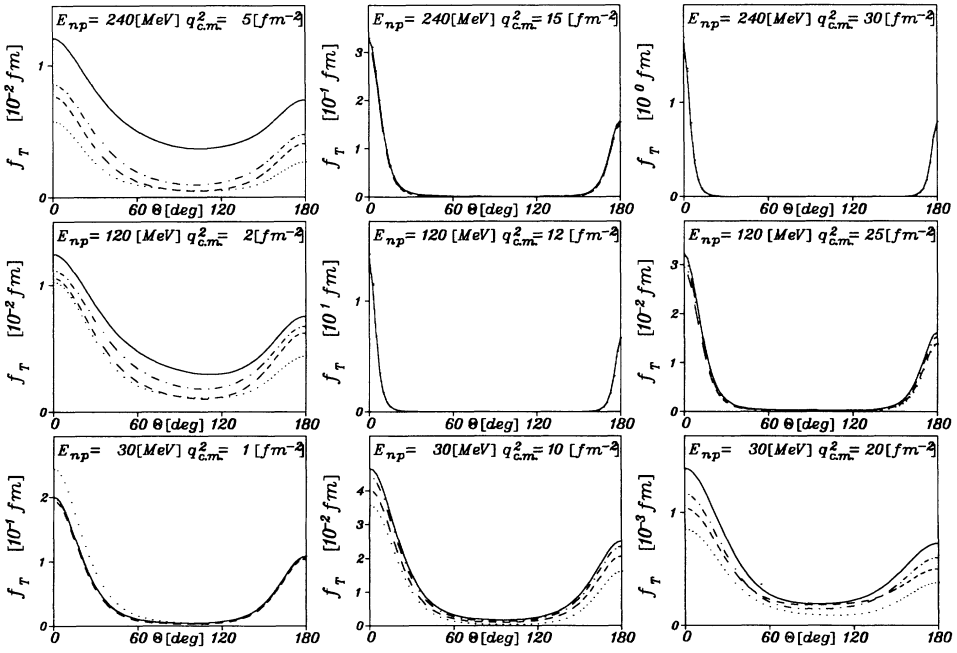

FIG. 4. The structure function f_T as function of θ in the kinematic sectors of Fig. 2. Ingredients and notation as in Fig. 3.

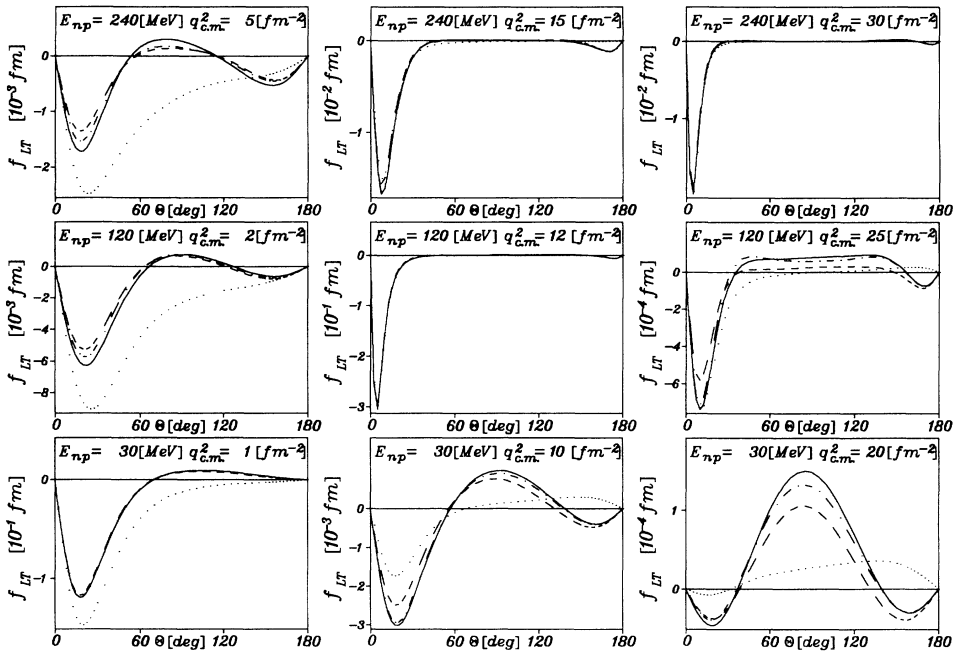

FIG. 5. The structure function f_{LT} as function of θ in the kinematic sectors of Fig. 2. Ingredients and notation as in Fig. 3.

backward direction corresponding to neutron emission along **q**. The reason for this is that the transverse current is dominated by the spin current in the quasifree case. Consequently, the ratio of the forward and backward peak heights are essentially given by the squared ratio of the proton to the neutron magnetic moments since the Born approximation is quite reliable. Away from the quasifree ridge final-state interactions and subnuclear d.o.f. become sizable in particular at low energy but higher momentum transfers (sectors Ib and Ic) and at higher energies at low momentum transfers (sectors IIa and IIIa). As expected for IIIa the IC effects are particularly strong.

The next two figures, 5 and 6, show the interference structure functions f_{LT} and f_{TT}, respectively: Both of them are more than an order of magnitude smaller than

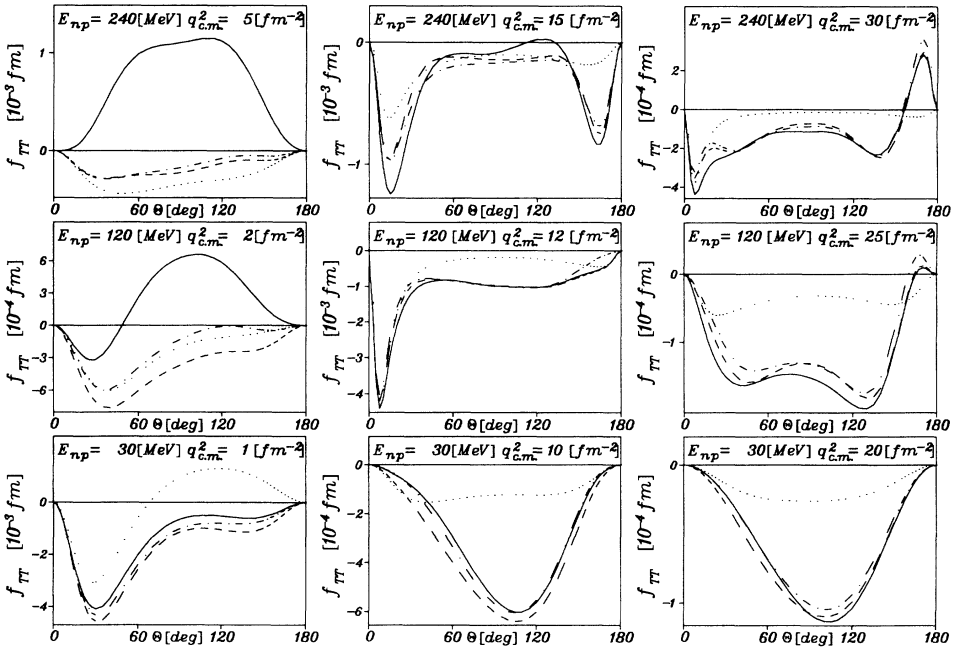

FIG. 6. The structure function f_{TT} as function of θ in the kinematic sectors of Fig. 2. Ingredients and notation as in Fig. 3.

the diagonal ones, i.e., f_L and f_T. The longitudinal-transverse function f_{LT} exhibits a strong forward peak in the quasifree case as well as at higher energies and momentum transfers. Only at low momentum transfers does one note an oscillatory behavior at all energies (sectors Ia, IIa, IIIa) although for the lowest energy this behavior also occurs at higher momentum transfers (sectors Ib and Ic). Here the final-state interaction is important and there is some sensitivity to MEC and—of lesser extent—to IC. The other interference function f_{TT} is in most kinematic sectors almost an order of magnitude smaller than f_{LT} except for the sectors Ic, IIc, and IIIa. Right on the quasifree ridge (IIb) it is even two orders of magnitude smaller. In general f_{TT} shows a much larger sensitivity to both final-state interactions and subnuclear d.o.f., in particular in the low momentum transfer sectors Ia–IIIa. One also notes a marked difference in the functional behavior of f_{TT} in the various kinematical sectors.

Now we will consider the "polarized" structure functions. In Fig. 7 we show in all kinematic sectors the fifth structure function f'_{LT} for a longitudinally polarized electron beam. According to Eq. (13) it is proportional to the imaginary part of v_{0100} and therefore, as is well known, vanishes in Born approximation due to Watson's final-state theorem. Thus, compared to f_{LT} it is almost an order of magnitude smaller at low and medium momentum transfers above the quasifree ridge. In this region f'_{LT} shows a similar angular behavior as f_{LT} except for a more pronounced forward neutron peak. Only at higher momentum transfers below the quasifree ridge (sectors IIc and IIIc) is it comparable in size although the angular behavior then is quite different. In the sectors Ia and IIa one notes also a greater sensitivity to IC contributions.

With respect to deuteron orientation we will first consider the diagonal structure function f_L^{IM} and $f_T^{IM}(I>0)$. In Fig. 8 we show these in sectors Ib, IIb, and IIIb for a vector polarized target. They vanish in Born approximation for the same reason as did f'_{LT} and, therefore, are as small in size. At low energy (sector Ib) one notes for f_L^{11} a rather broad minimum around 25° and a maximum around 110° while the opposite behavior is observed in f_T^{11}. With increasing energy both structure functions develop a pronounced minimum at small forward angles. However, while f_L^{11} exhibits a shallow minimum at backward angles, f_T^{11} shows another pronounced maximum of almost the same absolute size as its forward minimum. MEC and IC show in general very little influence even in the Δ region. The only exception is for f_T^{11} in sector Ib where a strong effect from explicit MEC beyond the Siegert operators is seen.

The corresponding structure functions for a tensor polarized deuteron target are shown in Figs. 9 and 10 again in the sectors, Ib, IIb, and IIIb. Compared to f_L the structure functions $f_L^{2M}(M=0,1,2)$ are roughly an order of magnitude smaller. The prominent feature is the pronounced maximum or minimum at small forward angles for higher energies (sectors IIb and IIIb). One notes some influence from final-state interactions but no effect from MEC and IC. This is not true for the corresponding transverse structure function f_T^{2M} $(M=0,1,2)$ where one readily sees some influence—mainly MEC beyond Siegert—in sector Ib and for f_T^{21} even in the quasifree case (sector IIb). Otherwise there is almost no sign of subnuclear degrees of freedom even in the Δ region.

Finally we show a few selected examples of further structure functions f_α^{IM} in Fig. 11 and $f_\alpha^{\prime IM}$ in Fig. 12 $(I>0)$ which are either quite large in size or which show a particularly strong sensitivity to final-state interaction,

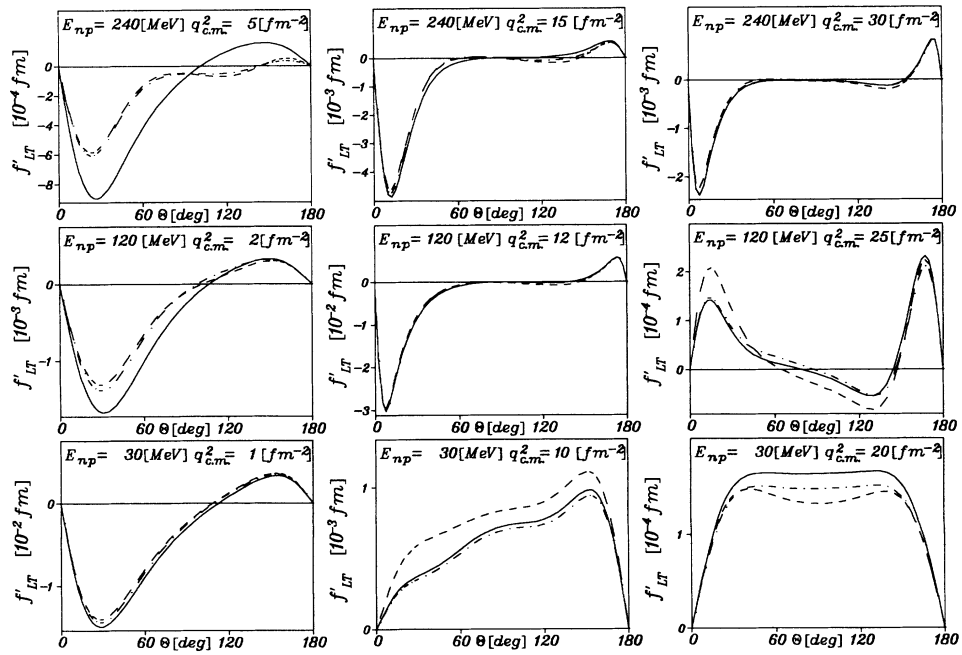

FIG. 7. The structure function f'_{LT} as function of θ in the kinematic sectors of Fig. 2. Ingredients and notation as in Fig. 3.

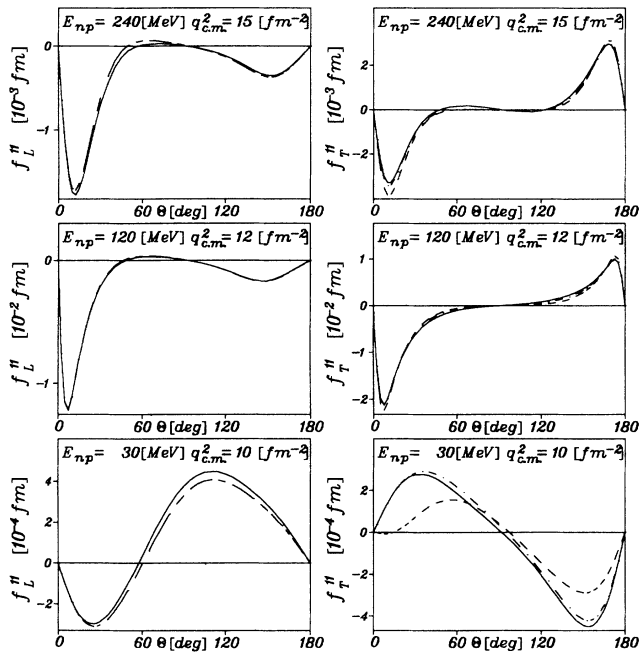

FIG. 8. The structure function f_L^{11} and f_T^{11} as function of θ in the kinematic sectors Ib, IIb, and IIIb of Fig. 2. Ingredients and notation as in Fig. 3.

MEC or IC. All examples in Fig. 11 and the two upper cases in Fig. 12 exhibit a strong influence from final-state interactions—f_{LT}^{10}, f_{TT}^{10}, and $f_T^{\prime 22}$ would even vanish without them—to MEC and IC. The two lower examples in Fig. 12 are comparable or even larger than f_{LT} and are insensitive to MEC and IC.

B. Potential model dependence

Just as in the last section we start the discussion by first showing the potential model dependence for the four "unpolarized" and the fifth structure functions in those sectors where it is relevant (Figs. 13 and 14). Apart from f_T (right side of Fig. 13) all of them exhibit interesting effects at least for a few kinematics. The longitudinal structure function (left side of Fig. 13), for example, is affected at proton forward angles at low momentum transfer (sectors IIa and IIIa) and here it is worth noting that one has the strongest deviations from other potential models for the CC with V_{28}. The two interference structure functions f_{LT} and f_{TT} and the fifth one f'_{LT} shown in Fig. 14 depend much more on the potential model than f_L. Here one finds the most significant effects again for the two sectors IIa and IIIa, but potential model dependence is present in other sectors as well. In particular, f_{TT} shows in almost all kinematic sectors quite large potential effects. It is interesting to note that f'_{LT} appears to be less sensitive to the potential model in sector IIIa than f_{LT} although it vanishes without final-state interaction. In general, these interference structure functions may thus serve as a test for the various NN interaction models. However, one should note that all of them, especially f_{TT}, receive subnuclear current contributions which have a size that is similar or even bigger than the size of the potential model dependence (see Figs. 5–7). It would of course be much better to have cases where the potential effects dominate all other effects. Polarization structure functions which best fulfill such a condition will be described in the following.

One may expect particularly strong potential model effects for those structure functions which vanish in Born

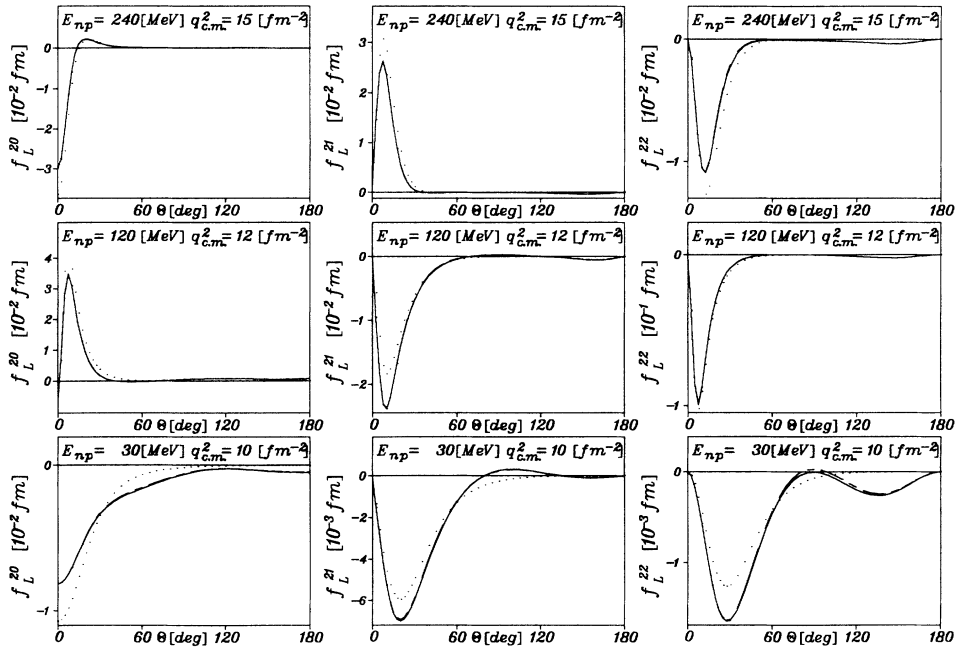

FIG. 9. The structure function f_L^{2M} ($M=0,1,2$) as functions of θ in the kinematic sectors Ib, IIb, and IIIb of Fig. 2. Ingredients and notation as in Fig. 3.

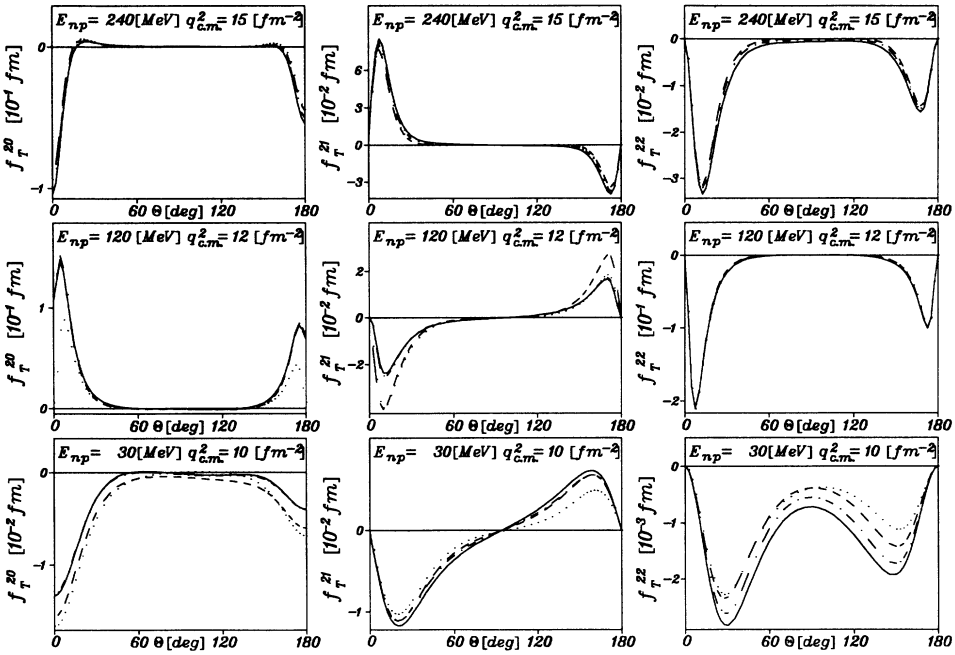

FIG. 10. The structure functions f_T^{2M} ($M=0,1,2$) as function of θ in the kinematic sectors Ib, IIb, and IIIb of Fig. 2. Ingredients and notation as in Fig. 3.

approximation. These are f_α^{1M} and $f_\alpha^{\prime 2M}$ according to Eqs. (12) and (13). Altogether there are 16 cases (one L-three T-, nine LT-, and three TT-structure functions). In fact all of them exhibit a potential model sensitivity. However, the T- and TT-structure functions are even more affected by subnuclear currents. Thus the best candidates for studying the potential model dependence are the L- and LT-structure functions. We will concentrate on the most interesting ones which are $f_{LT}^{\prime 21\pm}$, $f_{LT}^{11\pm}$, f_L^{11}, and $f_{LT}^{\prime 20}$. As described in the Appendix they can be experimentally determined by one $(f_{LT}^{11-}, f_{LT}^{\prime 20})$ or two $(f_{LT}^{\prime 21\pm}, f_{LT}^{11+}, f_L^{11})$ asymmetry measurements. Only in case of f_L^{11} one needs an additional Rosenbluth separation.

The structure function $f_{LT}^{\prime 21\pm}$ are strongly potential model dependent for a variety of kinematics. This is shown in Fig. 15 for $f_{LT}^{\prime 21+}$ (sectors IIa, IIb, IIIc) and for $f_{LT}^{\prime 21-}$ (sectors IIa, IIc, IIIb). Furthermore, we show in Fig. 16 in sector IIa the current contributions and the form factor effects. Comparing the results for the two structure functions in sector IIa it is evident that both of them are similarly influenced by the various potential

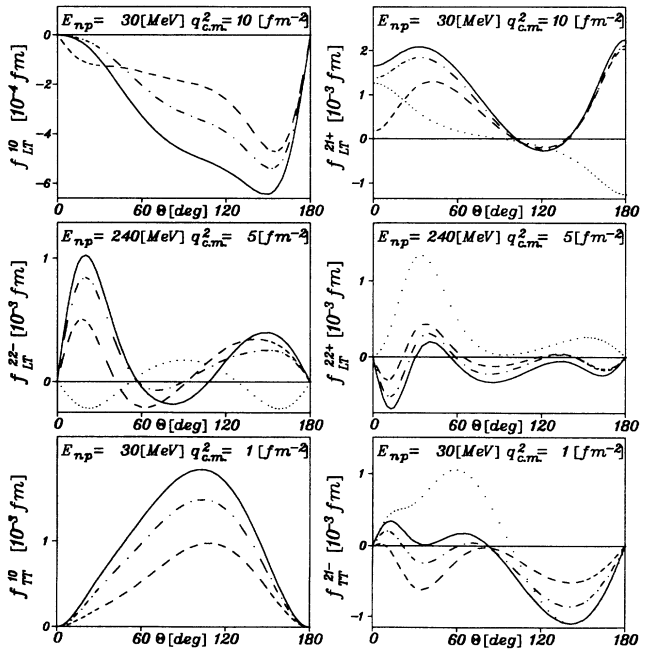

FIG. 11. Various structure functions f_{LT}^{IM} and f_{TT}^{IM} as function of θ in different kinematic sectors of Fig. 2. Ingredients and notation as in Fig. 3.

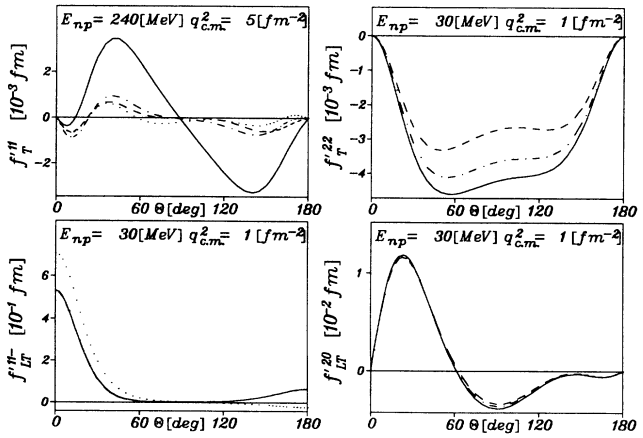

FIG. 12. Various structure function $f_\alpha^{\prime IM}$ as function of θ in different kinematic sectors of Fig. 2. Ingredients and notation as in Fig. 3.

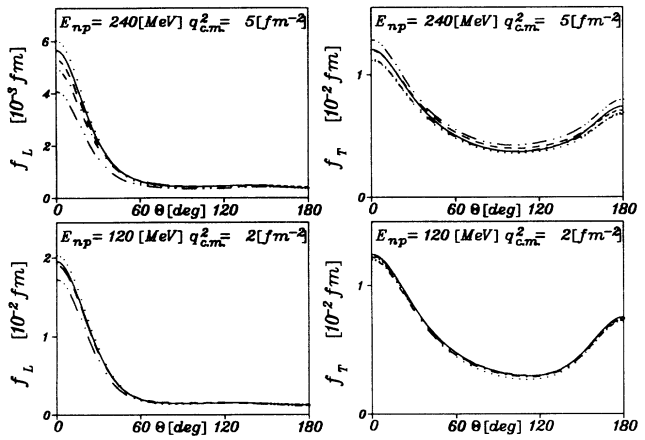

FIG. 13. Potential model dependence of the diagonal structure functions f_L and f_T as function of θ in the kinematic sectors IIa and IIIa. (MEC and IC included, dipole fit with $G_{En}=0$ for nucleon form factors, G_E^V as MEC form factor): Bonn (dotted curve), V_{14} (dashed curve), Nijmegen (dash-dotted curve), V_{28} (dash-double-dotted curve), and Paris (full curve) potentials.

models. In particular, one readily sees a very strong potential model dependence at forward and backward angles. Furthermore, one notes that form factor and subnuclear current effects are considerably less important and that for some of the shown cases, in particular at proton backward angles, these effects are even negligible. However, we would like to point out that this is not always true for the other sectors, especially at high momentum transfer (sectors Ic–IIIc).

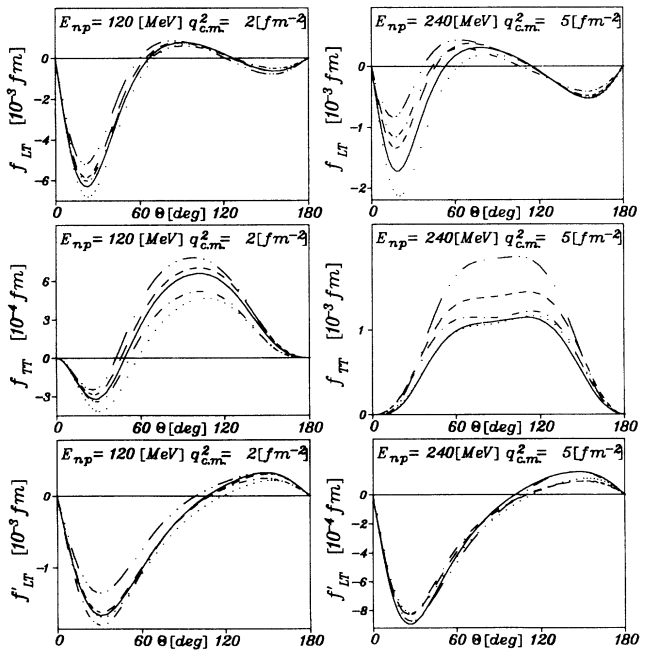

FIG. 14. Potential model dependence of the interference structure functions f_{LT}, f_{TT}, and the fifth structure function f'_{LT} as function of θ in the kinematic sectors IIa and IIIa. Ingredients and notation as in Fig. 13.

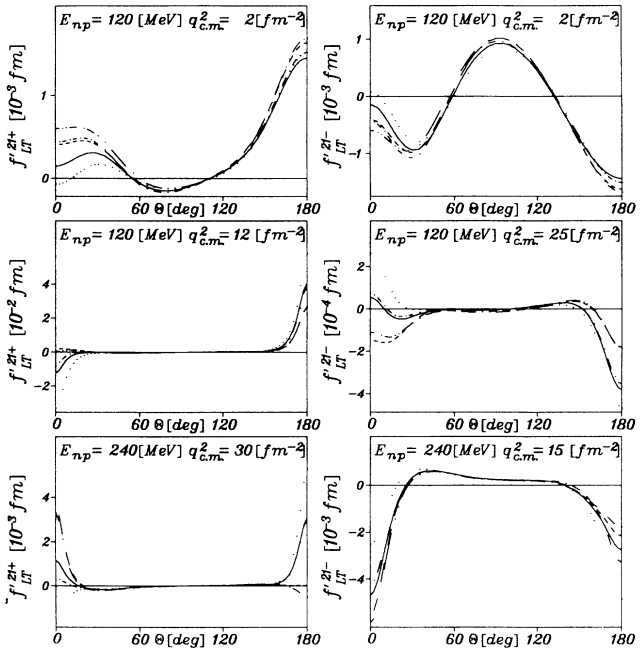

FIG. 15. Potential model dependence of the structure functions $f'^{21\pm}_{LT}$ as function of θ in the kinematic sectors IIa, IIb, and IIIc. Ingredients and notation as in Fig. 13.

Also the two structure functions $f^{11\pm}_{LT}$ are affected in a similar way by the various ingredients of our calculation. This is shown in Fig. 17 for altogether four kinematics (sectors Ia, IIa, IIb, IIIa). The strongest potential model effects are again present at forward and backward angles. Though form factor and subnuclear current influences—not shown here— are somewhat more important than for $f'^{21\pm}_{LT}$ the potential model dependence remains the

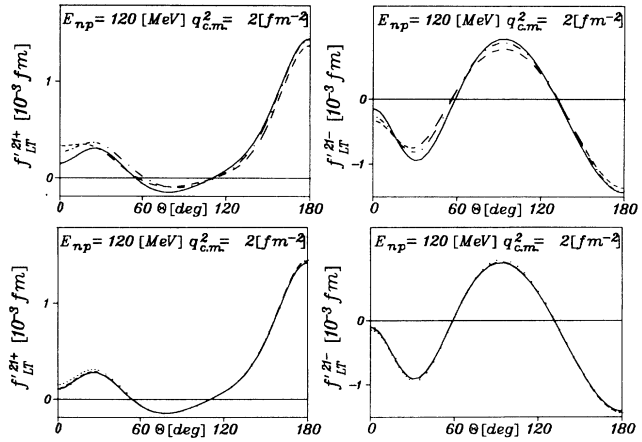

FIG. 16. The structure functions $f'^{21\pm}_{LT}$ as function of θ in the kinematic sector IIa. Current contributions (upper part, notation as in Fig. 3) and nucleon form factor dependence (lower part) with GK (full curve) and D (dashed curve) fits, and dipole fit with $G_{En}=0$ (dotted curve) (MEC and IC included, Paris potential, G_E^V as MEC form factor). Results with GK fit also for F_1^V as MEC form factor (dash-dotted curve).

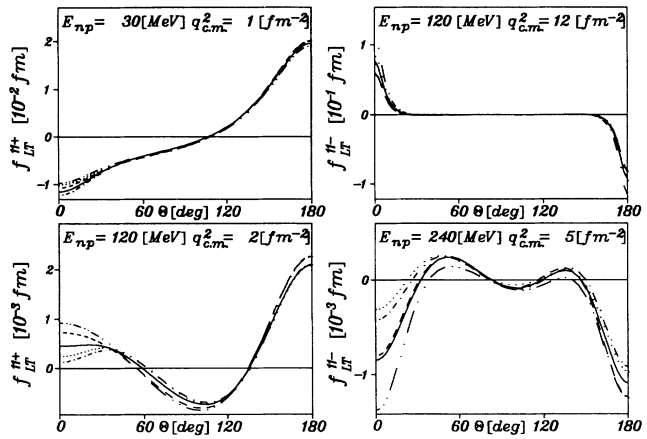

FIG. 17. Potential model dependence of the structure functions f_{LT}^{11+} and f_{LT}^{11-} as function of θ in various kinematic sectors. Ingredients and notations as in Fig. 13.

most prominent effect.

Our next case, the structure function f_L^{11}, exhibits a very interesting behavior for the kinematics IIa and IIIb as shown in Fig. 18. The various potential models lead to very different results for f_L^{11} for a rather large kinematical range which extends for proton angles between about 10° and 90° for kinematics IIa and between 10° and 60° for kinematics IIIb. Since all other model dependences remain very small, f_L^{11} seems to be very appropriate to study potential effects. However, as mentioned above, the experimental determination of f_L^{11} requires not only two asymmetry measurement but also a Rosenbluth separation. Results for the last of the above-mentioned six structure functions are also shown in Fig. 18 for two kinematics (sectors IIa and IIb). The potential model dependence is already considerably smaller than for the other five discussed cases. One finds the cleanest evidence of potential effects in the region of the second maximum for the kinematics IIa. For the other kinematics form factor effects have already a similar size as potential effects.

As last topic of this section we want to study to what extent explicit Δ-degrees of freedom in the interaction model do lead to a different behavior of a structure function. As already mentioned before, of all our potential models only V_{28} includes explicit Δ-degrees of freedom. Thus we have searched for structure functions where the results with V_{28} are rather different from the ones with the other potential models. The most interesting kinematics turns out to be sector IIIa, i.e., in the Δ resonance region at low momentum transfer, where one finds the largest effects and quite a number of cases. Choosing only structure functions where one or two asymmetry measurements are sufficient for an experimental determination we end up with four cases: f_{LT}^{22-}, $f_{TT}^{10/11-}$, and $f_T^{\prime 21}$. Their potential model dependence is shown in Fig. 19. It is evident that V_{28} leads for all these structure functions to a significantly different behavior compared to the other *NN* interaction models. Thus one may hope that an experimental study of these four cases might shed some light on the role of explicit Δ-degrees of freedom in the *NN* interaction.

C. Form factor effects

It is of interest to examine all 41 structure functions with regard to their sensitivity to nucleon electromagnetic form factors. In particular we are interested in determining which structure functions would be useful in determining G_{En}. Thus the structure functions have been calculated using the three above-mentioned models for the electromagnetic form factors: (i) the dipole fit [19] with $G_{En}=0$, (ii) the dipole fit of [19] using $p=5.6$, and (iii) the Gari-Krümpelmann model [20]. We refer to these here as the $G_{En}=0$, D, and GK models, respectively. In addition we have looked for those structure func-

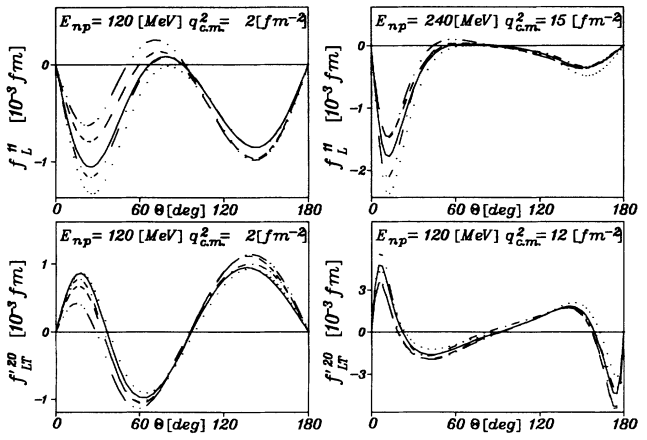

FIG. 18. Potential model dependence of the structure functions f_L^{11} (upper part, sectors IIa and IIIb) and $f_{LT}^{\prime 20}$ (lower part, sectors IIa and IIb) as function of θ. Ingredients and notations as in Fig. 13.

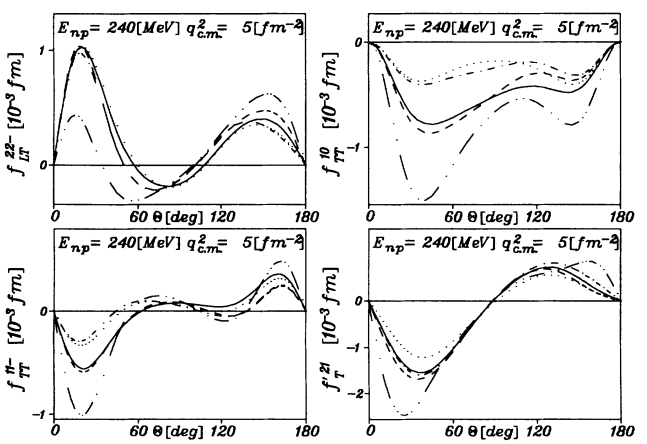

FIG. 19. Potential model dependence of the structure functions f_{LT}^{22-}, f_{TT}^{10}, f_{TT}^{11-}, and $f_T^{\prime 21}$. Ingredients and notation as in Fig. 13.

tions which might unambiguously differentiate between the effects of using G_E^V or F_1^V in the calculation of the meson-exchange currents. This issue has been discussed in detail in [21] with the conclusion that whenever one finds a sizable difference in results depending on which form factor is used, then a relativistic treatment is called for.

In order to be a good candidate for learning about nucleon form factors a structure function must not only be sensitive to such effects but must, in all other respects, be essentially model independent. We have examined the results of our calculations to see which structure functions satisfy these criteria. In most cases the criteria are met in only a few kinematical regions. Table I lists the structure functions which show sensitivity to G_{En} as well as model independence in the sectors indicated. We note that for all these structure functions the effect shows up either at $\theta=\pi$ or close to π. Figure 20 illustrates these effects for the structure functions f_L and f_L^{20} in the kinematical regions listed in Table I and for f_L^{21} in sector IIIc. The other structure functions listed in the table show similar effects.

It is not surprising to see the structure functions $f_{LT}^{\prime 11,\pm}$ listed in Table I since they play a dominant role in determining A_{ed}^V as discussed by us in an earlier publication [1]. In addition to the structure functions listed in Table I, there are others where the effect of G_{En} is somewhat weaker or where the model dependence is a little stronger. These are f_L^{11}, f_{LT}^{10}, and $f_{LT}^{\prime 20}$. For example, Fig. 21 shows that the structure function f_L^{11} has a strong G_{En} sensitivity not only at backward angles but even at forward angles in sectors IIIc and IIc. However, there is a strong potential model sensitivity at forward angles so that the measurement should be for the backward angles where the potential model dependence is weak. Also, whereas $f_{LT}^{\prime 20}$ shows a strong G_{En} dependence at forward angles in sectors IIIc and IIc, the potential model dependence is severe in sector IIIc and moderate in sector IIc. This is one of the only examples we could find where a measurement at forward angles of θ could give information on G_{En}.

Our search for a structure function which would help address the G_E^V-F_1^V controversy was less successful. Although many of the structure functions show a large difference depending on whether or not the exchange currents are computed using G_E^V or F_1^V, in many of these cases there is an equally large potential model dependence. There are a few cases, however, where the potential model dependence may be sufficiently weak to justify a measurement of the structure function, especially if the uncertainty in G_{En} has been removed by a measurement of, say, one of the structure functions listed in Table I. These are shown in Table II. As an illustration Fig. 22 shows that the structure function f_{LT}^{22+} has a strong sensitivity to the MEC form factor at both forward and backward directions.

With this we will conclude our first systematic survey of polarization effects in exclusive two-body electrodisintegration of the deuteron without polarization analysis of the outgoing nucleons. We hope that is will stimulate experimentalists to study this important process in greater detail in the future. An atlas of all structure functions showing the influence of currents, potential models, and form factor effects in various kinematical regions will be forthcoming.

TABLE I. Structure functions and kinematic regions with sensitivity to G_{En}.

Structure function	θ	Kinematic sector
f_L	π	IIc,IIIc
f_L^{20}	π	IIb,IIc,IIIc
f_L^{22}	$\approx\pi$	IIIc
f_L^{21}	$\approx\pi$	IIb,IIc,IIIc
f_{LT}	$\approx\pi$	IIIc
$f_{LT}^{\prime 11\pm}$	π	Ib,IIb,IIc,IIIb,IIIc
$f_{LT}^{\prime 10}$	$\approx\pi$	IIIb,IIIc

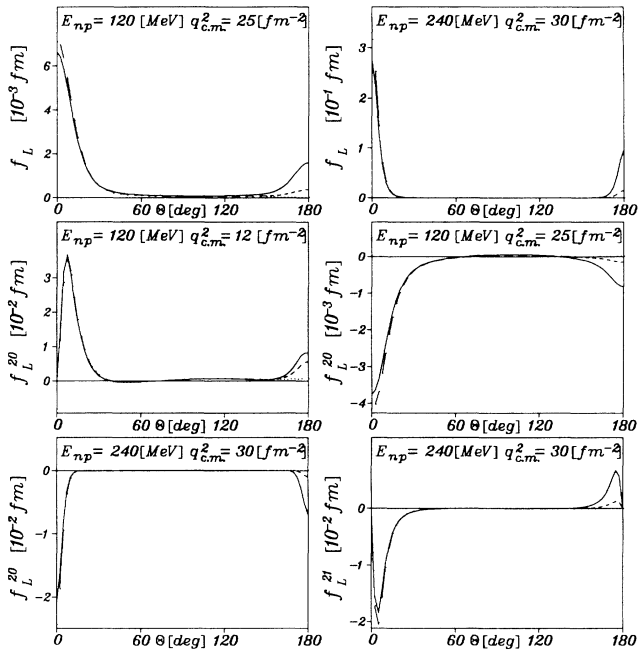

FIG. 20. Sensitivity of f_L, f_L^{20}, and f_L^{21} to the electric neutron form factor G_{En} in various kinematic sectors (Paris potential and G_E^V for MEC form factor). Dotted curves, dipole form factor with $G_{En}=0$; dashed, dipole form factor with $G_{En}\neq 0$, solid curves, GK form factors.

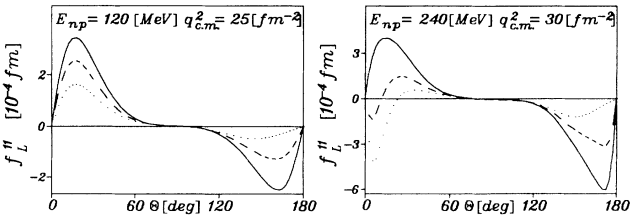

FIG. 21. Sensitivity of f_L^{11} to the electric neutron form factor G_{En}. Ingredients and notation as in Fig. 20.

TABLE II. Structure functions and kinematic regions with sensitivity to F_1^V.

Structure function	θ	Kinematic sector
f_T	π	IIc
f_{LT}^{22+}	≈ 0	IIIc
$f_{LT}^{\prime 20}$	≈ 0	IIc
f_{TT}^{10}	$\approx 2\pi/3$	Ib

ACKNOWLEDGMENTS

This work was supported in part by the Deutsche Forschungsgemeinschaft (S.F.B 201) and in part by the Natural Sciences and Engineering Research Council of Canada. Two of the authors (H. A. and W. L.) would like to thank the Saskatchewan Accelerator Laboratory for the hospitality extended to them during a visit.

APPENDIX

Here we describe an optimal way for separating a given structure function $f_\alpha^{IM(\pm)}$ $(I>0)$ and $f_\alpha^{\prime IM(\pm)}$. This is a different task than the complete separation of all structure functions as discussed in Sec. III. In fact, there we did not concern ourselves with the question of how many measurements are necessary for the separation of a specific structure function.

The first step in the determination of any structure function is the measurement of that asymmetry to which it contributes. This requires already a number of measurements with different electron and deuteron polarization parameters, i.e., two for A_e, A_d^V, and A_d^T and four for A_{ed}^V and A_{ed}^T. Next one must determine how many different settings of the angles ϕ, ϕ_d, and θ_d are necessary for the final separation. As one will see in the following, the structure functions can be divided into different classes according to the minimum number of asymmetry measurements required for their extraction. A quick glance at (30) through (34) shows that the five asymmetries contain differing numbers of structure functions, in detail, one in A_e, 8 in A_d^V, 16 in A_d^T, 5 in A_{ed}^V, and 7 in A_{ed}^T.

Obviously, the simplest case is the electron asymmetry A_e containing only $f_{LT}^{\prime}$. This means that $f_{LT}^{\prime}$ can be determined from just one asymmetry measurement. Similarly a close inspection of the dependence of the asymmetries on the angles ϕ, ϕ_d, and θ_d shows that four other structure functions and two combinations need only one asymmetry measurement, namely,

$$\rho_{LT} f_{LT}^{10} = S_d^V(\pi/2,\tilde{\phi},0) , \tag{A1}$$

$$\rho_{LT} f_{LT}^{11,-} = -\sqrt{2} S_d^V(\pi/2,\tilde{\phi},\pi/2) , \tag{A2}$$

$$\rho_T^{\prime} f_T^{\prime 10} = S_{ed}^V(\pi/2,0,0) , \tag{A3}$$

$$\rho_T^{\prime} f_T^{\prime 11} = -\sqrt{2} S_{ed}^V(\pi/2,0,\pi/2) , \tag{A4}$$

$$\rho_{LT}^{\prime} f_{LT}^{\prime 11,+} = \sqrt{2} S_{ed}^V(\pi/2,\pi/2,\pi/2) , \tag{A5}$$

$$\rho_{LT}^{\prime} f_{LT}^{\prime 20} = S_{ed}^T(\pi/2,\tilde{\phi},0) , \tag{A6}$$

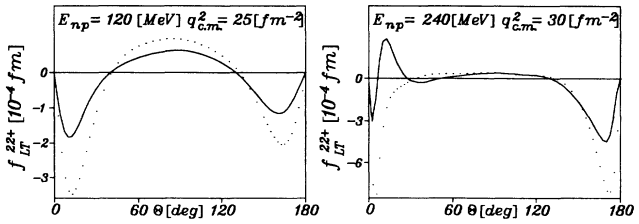

FIG. 22. Sensitivity of f_{LT}^{22+} to the MEC form factors G_E^V and F_1^V. Ingredients as in Fig. 20 with GK form factors. Dotted curves, F_1^V as MEC form factor; solid curves, G_E^V as MEC form factor.

where we have introduced for convenience in order to explicitly exhibit the angular dependence

$$S_{d/ed}^{V/T}(\phi,\tilde{\phi},\theta_d) = S_0(\phi) A_{d/ed}^{V/T}(\phi,\tilde{\phi},\theta_d) . \tag{A7}$$

Six other structure functions and seven combinations require only two measurements for their separation. These are

$$\rho_{TT} f_{TT}^{10} = \frac{2}{\sqrt{3}} S_d^V(\pi/3,\tilde{\phi},0) - S_d^V(\pi/2,\tilde{\phi},0) , \tag{A8}$$

$$\rho_{LT} f_{LT}^{11,+} = -[S_d^V(\pi/4,\pi/2,\pi/2) - S_d^V(3\pi/4,\pi/2,\pi/2)] , \tag{A9}$$

$$\rho_{TT} f_{TT}^{11,-} = -\sqrt{\tfrac{2}{3}}[2S_d^V(\pi/3,0,\pi/2) - \sqrt{3} S_d^V(\pi/2,0,\pi/2)] , \tag{A10}$$

$$\rho_{LT} f_{LT}^{20} = \frac{1}{\sqrt{2}}[S_d^T(\pi/4,\tilde{\phi},0) - S_d^T(3\pi/4,\tilde{\phi},0)] , \tag{A11}$$

$$\rho_{LT} f_{LT}^{21,-} = \frac{\sqrt{3}}{2}[S_d^T(\pi/2,\pi/2,\theta_d^0) - S_d^T(\pi/2,-\pi/2,\theta_d^0)] , \tag{A12}$$

$$\rho_{LT} f_{LT}^{22,-} = -\sqrt{\tfrac{2}{3}}[2S_d^T(\pi/2,\pi/4,\pi/2) + S_d^T(3\pi/2,\pi/4,0)] , \tag{A13}$$

$$\rho_{LT}^{\prime} f_{LT}^{\prime 10} = S_{ed}^V(0,\tilde{\phi},0) - S_{ed}^V(\pi/2,\tilde{\phi},0) , \tag{A14}$$

$$\rho_{LT}^{\prime} f_{LT}^{\prime 11,-} = -\sqrt{2}[S_{ed}^V(0,0,\pi/2) - S_{ed}^V(\pi/2,0,\pi/2)] , \tag{A15}$$

$$\rho_T^{\prime} f_T^{\prime 21} = -\frac{\sqrt{3}}{2}[S_{ed}^T(0,\pi/2,\theta_d^0) + S_{ed}^T(\pi,\pi/2,\theta_d^0)] , \tag{A16}$$

$$\rho_T^{\prime} f_T^{\prime 22} = \sqrt{\tfrac{2}{2}}[2S_{ed}^T(\pi/2,\pi/4,\pi/2) + S_{ed}^T(\pi/2,\pi/4,0)] , \tag{A17}$$

$$\rho_{LT}^{\prime} f_{LT}^{\prime 21,-} = -\frac{\sqrt{3}}{2}[S_{ed}^T(0,\pi/2,\theta_d^0) - S_{ed}^T(\pi,\pi/2,\theta_d^0)] , \tag{A18}$$

$$\rho_{LT}^{\prime} f_{LT}^{\prime 21,+} = -\frac{\sqrt{3}}{2}[S_{ed}^T(\pi/2,0,\theta_d^0) - S_{ed}^T(\pi/2,\pi,\theta_d^0)] , \tag{A19}$$

$$\rho'_{LT} f'^{22,+}_{LT} = \sqrt{\tfrac{3}{2}}[S^T_{ed}(\pi/2,0,\theta^0_d) + S^T_{ed}(\pi/2,\pi,\theta^0_d)] \tag{A20}$$

$$= \sqrt{\tfrac{2}{3}}[2S^T_{ed}(\pi/2,0,\pi/2) + S^T_{ed}(\pi/2,0,0)] \, . \tag{21}$$

The terms $\rho_L f^{11}_L + \rho_T f^{11}_T$ in A^V_d and $\rho_L f^{20}_L + \rho_T f^{20}_T$ in A^T_d can also be determined from two asymmetry measurements, i.e.,

$$\rho_L f^{11}_L + \rho_T f^{11}_T = -\frac{1}{\sqrt{2}}[S^V_d(\pi/4,\pi/2,\pi/2) + S^V_d(3\pi/4,\pi/2,\pi/2)] \, , \tag{A22}$$

$$\rho_L f^{20}_L + \rho_T f^{20}_T = \tfrac{1}{2}[S^T_d(\pi/4,\tilde{\phi},0) + S^T_d(3\pi/4,\tilde{\phi},0)] \, . \tag{A23}$$

In order to separate the longitudinal from the transverse part one needs in addition a Rosenbluth analysis.

Increasing the number of asymmetry measurements to three allows one to determine only one further structure function and one combination, namely,

$$\rho_{TT} f^{11,+}_{TT} = -\frac{1}{\sqrt{2}}[S^V_d(\pi/4,\pi/2,\pi/2) + S^V_d(3\pi/4,\pi/2,\pi/2) + 2S^V_d(\pi/2,\pi/2,\pi/2)] \, , \tag{A24}$$

$$\rho_{TT} f^{20}_{TT} = \tfrac{1}{2}[S^T_d(\pi/4,\tilde{\phi},0) + S^T_d(3\pi/4,\tilde{\phi},0)] - S^T_d(\pi/2,\tilde{\phi},0) \, . \tag{A25}$$

All thirteen vector structure functions are then determined and twelve of the tensor ones or respective combinations. For the remaining combination $f^{21,+}_{LT}$, $f^{22,+}_{LT}$, $f'^{22,-}_{LT}$, $f^{21,-}_{TT}$ $f^{22,-}_{TT}$, $(\rho_L f^{21}_L + \rho_T f^{21}_T)$, and $(\rho_L f^{22}_L + \rho_T f^{22}_T)$ one needs four measurements in order to determine them. The last two combinations require a Rosenbluth separation in addition. Finally, there remain two combination $f^{21,+}_{TT}$ and $f^{22,+}_{TT}$, where six settings are necessary.

[1] W. Leidemann, E. L. Tomusiak and H. Arenhövel, Phys. Rev. C **43**, 1022 (1990).
[2] H. Arenhövel, Nucl. Phys. **A384**, 287 (1982).
[3] A. Yu. Korchin, Yu. P. Mel'nik, and A. V. Shebeko, Few-Body Syst. **9**, 211 (1990).
[4] M. V. Tokarev, Few-Body Syst. **4**, 133 (1988).
[5] V. A. Karmanov, Lebedev Physics Institute Report 74, Moscow, 1989.
[6] W. Fabian and H. Arenhövel, Nucl. Phys. **A314**, 253 (1979).
[7] H. Arenhövel, Phys. Lett. B **199**, 12 (1987).
[8] H. Arenhövel, W. Leidemann, and E. L. Tomusiak, Z. Phys. A **331**, 123 (1988); **334**, 363(E) (1989).
[9] H. Arenhövel, Nucl. Phys. **A358**, 263c (1981).
[10] B. A. Robson, *The Theory of Polarization Phenomena* (Clarendon, Oxford, 1974).
[11] H. Arenhövel, Few-Body Syst. **4**, 55 (1988).
[12] H. Arenhövel and M. Sanzone, Few-Body Syst., Suppl. **3**, 1 (1991).
[13] F. Partovi, Ann. Phys. (N.Y.) **27**, 79 (1964).
[14] M. M. Nagels, T. A. Rijken, and J. J. de Swart, Phys. Rev. D **17**, 768 (1978).
[15] M. Lacombe, B. Loiseau, J. M. Richard, R. Vinh Mau, J. Côté, P. Pirès, and R. de Tourreil, Phys. Rev. C **21**, 861 (1980).
[16] R. Machleidt, K. Holinde, and Ch. Elster, Phys. Rep. **149**, 1 (1987).
[17] R. W. Wiringa, R. Smith, and T. L. Ainsworth, Phys. Rev. C **29**, 1207 (1984).
[18] W. Leidemann and H. Arenhövel, Nucl. Phys. **A465**, 573 (1987); P. Wilhelm, W. Leidemann, and H. Arenhövel, Few-Body Syst. **3**, 111 (1988).
[19] S. Galster, H. Klein, J. Moritz, K. H. Schmidt, D. Wegener, and J. Bleckwenn, Nucl. Phys. **B32**, 221 (1971).
[20] M. Gari and W. Krümpelmann, Z. Phys. A **322**, 689 (1985).
[21] S. K. Singh, W. Leidemann, and H. Arenhövel, Z. Phys. A **331**, 509 (1988).